UC Irvine
UC Irvine Previously Published Works

Title

Opposite Responses of the Dry and Moist Eddy Heat Transport Into the Arctic in the PAMIP Experiments

Permalink

https://escholarship.org/uc/item/2wm9w9d6

Journal

Geophysical Research Letters, 48(9)

ISSN

0094-8276

Authors

Audette, Alexandre
Fajber, Robert A
Kushner, Paul J
et al.

Publication Date

2021-05-16

DOI

10.1029/2020gl089990

Copyright Information

Peer reviewed

Geophysical Research Letters

Key Points:
- Sea ice loss exports static energy from the Arctic by warming the equatorward branch of the global mass circulation
- Sea surface warming imports static energy into the Arctic by increasing the mid-latitude mass transport, overwhelming the sea ice effect
- There is more spread amongst models for the effect of sea-surface warming than for sea ice loss

Supporting Information:

Supporting Information may be found in the online version of this article.

Correspondence to:

A. Audette,
alexandre.audette@utoronto.ca

Opposite Responses of the Dry and Moist Eddy Heat Transport Into the Arctic in the PAMIP Experiments

Alexandre Audette[1] , **Robert A. Fajber[1]** , **Paul J. Kushner[1]** , **Yutian Wu[2]** , **Yannick Peings[3]** , **Gudrun Magnusdottir[3]** , **Rosie Eade[4]** , **Michael Sigmond[5]** , and **Lantao Sun[6]**

[1]Department of Physics, University of Toronto, Toronto, ON, Canada, [2]Lamont–Doherty Earth Observatory, Columbia University, Palisades, NY, USA, [3]Department of Earth System Science, University of California, Irvine, CA, USA, [4]Met Office Hadley Centre, Exeter, UK, [5]Canadian Centre for Climate Modelling and Analysis, Environment and Climate Change, Victoria, BC, Canada, [6]Department of Atmospheric Science, Colorado State University, Fort Collins, CO, USA

Abstract Given uncertainty in the processes involved in polar amplification, elucidating the role of poleward heat and moisture transport is crucial. The Polar Amplification Model Intercomparison Project (PAMIP) permits robust separation of the effects of sea ice loss from sea surface warming under climate change. We utilize a moist isentropic circulation framework that accounts for moisture transport, condensation, and eddy transport, in order to analyze the circulation connecting the mid-latitudes and the Arctic. In PAMIP's atmospheric general circulation model experiments, prescribed sea ice loss reduces poleward heat transport (PHT) by warming the returning moist isentropic circulation at high latitudes, while prescribed warming of the ocean surface increases PHT by strengthening the moist isentropic circulation. Inter-model spread of PHT into the Arctic reflects the tug-of-war between sea-ice and surface-warming effects.

Plain Language Summary A major conundrum in current climate science is to understand what Arctic changes imply for the climate and environment in mid-latitude regions. The Polar Amplification Model Intercomparison Project (PAMIP) designed a set of climate model experiments to specifically answer this question in a carefully designed, idealized framework. PAMIP's approach is to separate historic and projected climate change into parts associated with Arctic sea ice loss and ocean surface warming and investigate how these two contributions can influence the atmosphere. To isolate these effects, only models can be used, because, in reality, sea ice loss and ocean surface warming are strongly linked together. This letter focuses on what the PAMIP experiments imply for the transport and redistribution of heat and moisture in the atmosphere. In PAMIP, we learn that Arctic sea ice loss causes the atmosphere to reduce the transport of dry and cold air away from the Arctic while ocean warming causes more transport of moist warm air toward the Arctic. These two effects are in a tug-of-war, suggesting that climate change can cause a mix of competing impacts on the global energy transport from the tropics to the Arctic.

1. Introduction

Radiative driving of the climate system tends to warm already warm regions such as the tropical lower troposphere, and cool already cold regions such as the high latitude troposphere and the upper atmosphere (Vallis et al., 2015). Poleward heat transport (PHT) works toward energy balance by moving heat from warmer to colder regions (e.g., Held, 2001; Trenberth & Stepaniak, 2003), primarily via atmospheric but also via oceanic pathways (Czaja & Marshall, 2006; Held, 2001). Atmospheric warming from anthropogenic climate change is also spatially varying, for example, in tropical upper- and Arctic lower-tropospheric warming (e.g., Deser et al., 2016; Vallis et al., 2015), which entails changes to PHT that also occur via the atmospheric pathway (e.g., Alexeev & Jackson, 2013; Barpanda & Shaw, 2020; Hwang & Frierson, 2010; Hwang et al., 2011; Shaw et al., 2018). Changes in PHT in observations have also been linked to reduced reflected shortwave radiation due to sea ice loss to reduced high-latitude PHT (Hartmann & Ceppi, 2014).

PHT responses to anthropogenic climate change involve tradeoffs between dry static energy and latent heat transport (Caballero & Langen, 2005; Döös & Nilsson, 2011; Frierson et al., 2007; Held & Soden, 2006).

The increase in atmospheric moisture content due to global warming increases total PHT (Hwang & Frierson, 2010), while polar amplification of global warming decreases PHT at high latitudes (Armour et al., 2019). Net changes in PHT into the Arctic have been shown to be relatively small due to a compensation between increased poleward latent heat flux and decreased poleward sensible heat flux (Hwang et al., 2011; Kay et al., 2012). This compensation highlights the important role that moisture plays in the structure of Arctic warming. Broadly, improving our understanding of the PHT response to global warming is an important part of advancing understanding of the mechanisms of polar amplification, which remain unsettled (Shaw & Tan, 2018; Smith et al., 2019; Stuecker et al., 2018).

The Polar Amplification Model Intercomparison Project (PAMIP, Smith et al., 2019), which is part of the sixth phase of the Coupled Model Intercomparison Project (CMIP6, Eyring et al., 2016), uses coordinated model experiments to separate the effects of global surface warming from Arctic sea ice loss on the process of polar amplification. This permits a thorough investigation of the role of sea ice loss in various aspects of the atmospheric response to anthropogenic climate change, including changes in climate extremes and the nature of teleconnected responses. However, PAMIP also provides a unique tool for investigating how global surface warming and sea ice loss separately impact atmospheric PHT.

To demonstrate insights to be gained into atmospheric PHT changes with this framework, we use PAMIP's recently completed atmosphere-land general circulation model (AGCM) simulations that are driven by the projected response of sea surface temperature (SST) and Arctic sea ice concentration (SIC) to future radiative forcing. The AGCM framework isolates atmospheric PHT changes in the absence of ocean coupling, and thus does not fully address the energy budget response in the coupled system. But this configuration is simple enough to efficiently attribute changes to atmospheric PHT to specific changes at the surface. This study only provides a starting point for understanding the effect of changes in PHT on the Arctic and tropical temperatures. A significant limitation is, therefore, that the feedback of these changes onto surface temperature responses cannot be assessed within the AGCM simulations in the Tier 1 PAMIP experiments that have been executed thus far.

This study focuses on eddy PHT since most of the atmospheric energetic transport is accomplished by eddies in the mid and high latitudes. We separate moist energetic from transport responses (Pauluis et al., 2010) and poleward-branch from equatorward-branch responses of the atmospheric overturning circulation, which exhibit distinctive PHT responses. Our analysis is centered on a moist thermodynamic framework that uses second order statistics computed from the simulations' output (Pauluis et al., 2011). This framework explicitly separates the distinctive dynamical responses of the poleward and the equatorward branches of the atmospheric overturning circulation, which aids in the interpretation of the PHT response.

Section 2 of this study describes the experiments from the PAMIP protocol and the different models used as well as the methods. Results are presented in Section 3, and Section 4 concludes by highlighting the main points of this paper.

2. Models and Methods

2.1. PAMIP Experiments and Models

Six AGCM groups (CanAM5, ECHAM6, EAM, CAM6, WACCM4, and GA7.1) (see Table S1, Golaz et al., 2019; Hewitt et al., 2011; Lauritzen et al., 2018; Marsh et al., 2013; Stevens et al., 2013; Swart et al., 2019) carried out experiments PAMIP 1.1, PAMIP 1.4 and PAMIP 1.6 (described below) and provided wind, temperature, geopotential height, and specific humidity data sampled on a daily or 6-hourly basis for our analysis.

The control experiment PAMIP 1.1 uses year 2000 SIC and SST; the sea ice loss experiment PAMIP 1.6 also uses year 2000 SST but with Arctic SIC projected to a 2°C global warming scenario relative to pre-industrial conditions (1.4°C compared to year 2000); and the sea surface warming experiment PAMIP 1.4 uses year 2000 SIC but with SST projected to the same 2°C patterned warming scenario as the sea ice in PAMIP 1.6. In PAMIP 1.6, where ocean is newly exposed due to sea ice loss, the SST is determined following Screen et al. (2012), that is, future SST are imposed in grid points where the SIC is at least 10% less than the present-day value. Both the imposition of future SSTs in the Arctic and sea ice loss in the PAMIP 1.6 experiment contribute to Arctic warming. In all PAMIP experiments, the atmospheric composition, and hence external

radiative forcing, is held fixed. The simulations were carried out in a time slice fashion: For every model, an ensemble of 100 members with different initial conditions was created, each individual simulation was integrated for 14 months, and the last 12 months were used for the analysis (Smith et al., 2019). These simulations isolate the rapid atmosphere-land adjustment in the absence of long-timescale oceanic/sea ice adjustments, and, as stated in Section 1, do not allow for additional oceanic/sea ice feedbacks.

2.2. Diagnostics of Poleward Heat Transport

The total climatological mean atmospheric PHT (H) can be written as the sum of a mean and an eddy term, but in the mid and high latitudes, the eddy contribution dominates (Trenberth & Stepaniak, 2003). The eddy PHT (H_E) can be expressed as

$$H_E(\phi) = \frac{2\pi a \cos\phi}{g} \int_0^{p_s} \overline{\left[v^* h^*\right]} \, dp,$$

(1)

where h is used to represent either dry static energy (DSE $\equiv c_p T + gz$) or moist static energy (MSE $\equiv$ DSE $+ L_v q$), where T is the air temperature, z is the height, q is the specific humidity, c_p is the specific heat capacity at constant pressure of dry air, g is the gravitational acceleration and L_v is the latent heat of vaporization of water. The annual climatological mean is denoted by an overbar, the zonal mean by square brackets, and the departure from the zonal mean by $*$. The latitude is ϕ, a is the radius of Earth, p_s is the surface pressure and p is the pressure.

Additional insight into the eddy PHT response can be gained using the *moist isentropic circulation framework* (Fajber et al., 2018; Pauluis et al., 2010; Wu & Pauluis, 2012). This framework effectively maps the meridional mass flux onto isentropic coordinates (here, MSE coordinates), in which diabatic processes (here, processes that violate the pseudoadiabatic assumption) result in cross-isentropic (cross-MSE levels) mass fluxes. We describe, first, how mass transport in MSE coordinates can be approximated with a practical diagnostic and second, how the framework can be used to explicitly separate poleward and equatorward contributions as well as dynamical and thermodynamical contributions to the PHT.

In this moist isentropic perspective, the eddy PHT is given by

$$H_E(\phi) = \int_0^\infty \tilde{h} M_E(\phi, \tilde{h}) \, d\tilde{h},$$

(2)

where $\tilde{h}$ is the MSE coordinate and M_E is the eddy moist isentropic mass flux. This expression of the eddy PHT is equivalent to Equation 1.

The isentropic eddy mass flux can be obtained through a binning process (Pauluis et al., 2010) or through a statistical parametrization (Pauluis et al., 2011). We will use the latter in this study because of its practicality. This parametrization is the *statistical transformed eulerian mean* (STEM, Pauluis et al., 2011; Wu & Pauluis, 2012) and approximates the moist isentropic eddy mass flux (M_E) using second order eddy statistics of h and v (i.e., $\overline{\left[h\right]}$, $\overline{\left[v^* h^*\right]}$, $\overline{\left[h^{*2}\right]}$),

$$M_E(\phi, \tilde{h}) = \frac{2\pi a \cos\phi}{g} \int_0^{p_s} \frac{\overline{\left[v^* h^*\right]}(\tilde{h} - \overline{[h]})}{\sqrt{2\pi}\,\overline{[h^{*2}]}^{3/2}} \exp\left(\frac{-(\tilde{h} - \overline{[h]})^2}{2\overline{[h^{*2}]}}\right) dp.$$

(3)

The STEM is a generalization of the classical transformed eulerian mean (TEM) that is based on a statistical interpretation of the meridional circulation and the eddy statistics (Pauluis et al., 2011).

Additionally, expressing the eddy mass flux in a MSE-latitude coordinate space allows for the calculation of the eddy moist isentropic mass streamfunction ψ_E in this coordinate space (see Pauluis et al., 2011, for more details),

$$\psi_E(\phi, h) = \int_0^h M_E(\phi, \tilde{h}) \, d\tilde{h}.$$

(4)

This stream function provides insight about the eddy induced air-mass advection and changes to heat content.

In addition to providing a different view on the mass transport, the moist isentropic framework allows for a clear separation between the poleward and equatorward mass transports (Laliberté et al., 2012). This separation is achieved here by defining *indicator functions* $I_+(h, \phi)$ and $I_-(h, \phi) = 1 - I_+(h, \phi)$; defined so that I_+ is 0 where the mass flux is equatorward (i.e., where $M_E < 0$) and 1 where it is poleward. Conversely, I_- is 0 for poleward and 1 for equatorward mass flux. Then

$$F_{E\pm}(\phi) = \int_0^\infty M_E(\tilde{h}, \phi) I_\pm d\tilde{h},$$ (5)

are the poleward and equatorward eddy mass transports and

$$H_{E\pm}(\phi) = \int_0^\infty \tilde{h} M_E(\tilde{h}, \phi) I_\pm d\tilde{h},$$ (6)

are the poleward and equatorward heat transports.

In contrast with Laliberté et al. (2012), we apply mass conservation, which requires that at each latitude $F_{E+}(\phi) = -F_{E-}(\phi)$, so we define $F_E(\phi) \equiv |F_{E+}(\phi)| = |F_{E-}(\phi)|$. We can then define effective moist static energies for the poleward and equatorward branches, $h_\pm(\phi) \equiv H_{E\pm}(\phi)/F_E(\phi)$. By construction,

$$H_E = H_{E+} - H_{E-} = F_E(h_+ - h_-);$$ (7)

in this expression $(h_+ - h_-)$ is an effective moist stratification, similar to the effective stratification defined by Pauluis et al. (2010). This effective stratification is a measure of the ability of the circulation to transport moist static energy (Pauluis et al., 2010). Then, any change in H_E can be decomposed into changes in mass transport (F_E) and in effective moist static energy of the poleward branch (h_+) and equatorward branch (h_-),

$$\delta H_E \approx (h_+ - h_-)\delta F_E + F_E\delta h_+ - F_E\delta h_-,$$ (8)

where we neglect the second order term $(\delta h_+ - \delta h_-)\delta F_E$ (shown in Figure S1). The term $(h_+ - h_-)\delta F_E$ is the change in heat transport due to the change in mass transport and is associated with the dynamical response. The term $F_E\delta h_+$ is the change in heat transport due the change in the effective moist energy of the poleward branch, and the term $-F_E\delta h_-$ is the corresponding change for the equatorward branch. The sum of the last two terms in Equation 10 is the effect of changes in the effective stratification and are interpreted as the thermodynamic response.

The statistical significance of the results is assessed with a local Student t-test assuming that individual realizations of the models are independent. To account for potential biases in the strength of the response to different climatologies, the individual ensemble mean of each model was removed. A p-value of 0.05 or less was chosen to determine significance.

3. Results and Discussion

3.1. Surface Response to PAMIP Boundary Forcings

In response to Arctic sea ice loss, all models show an increase of the zonal-mean near-surface (lowest model level) DSE and MSE at high latitudes (Figure 1b and see Figure S2 for the individual models). The climatology is shown in Figure 1a for reference. Although the forcing is the same for all models, the amplitude of the maximal Arctic amplification signal (the maximum difference in MSE increase between the Arctic and the tropics) varies substantially, with a multi-model mean of 3.5 kJ kg^{-1} and an inter-model spread (maximum − minimum) of 2.0 kJ kg^{-1} for surface MSE. The cause of this spread in the degree of Arctic amplification, which is present even with a highly constrained and consistent forcing like the SIC perturbation of PAMIP, is as yet undetermined. One potential source of model spread is from differences in the models' cloud parametrization as cloud radiative feedbacks have a significant effect on Arctic Amplification (Kim et al., 2018). We argue in Section 3.2 that this spread seems to have little bearing on the eddy PHT responses to sea ice loss. Moreover, most of the signal in MSE is coming from an increase in surface DSE, the latent heat response (MSE − DSE) being relatively weak.
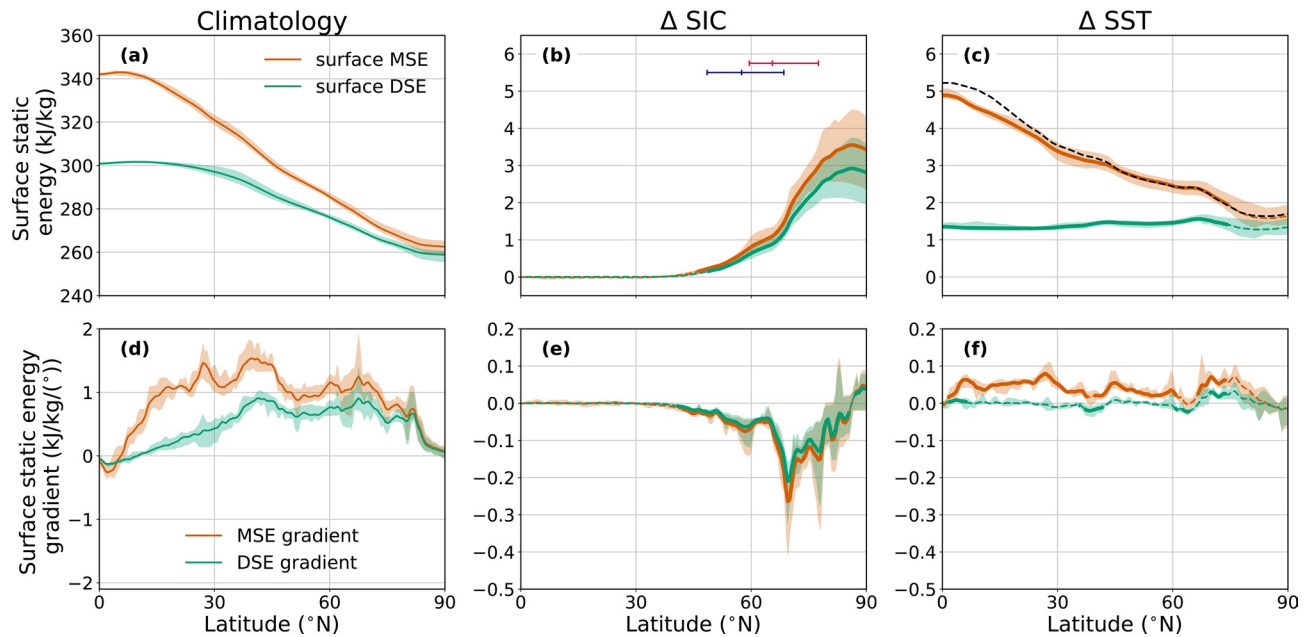
Figure 1. Annual, zonal and multi-model mean surface static energy. (a) Climatology of the annual and zonal mean surface MSE (orange) and DSE (green). (b) Response of the surface MSE and DSE to Arctic sea ice loss. The minimum, mean and maximum sea ice extent are shown in (b) by the blue (present day) and red (future) horizontal lines. (c) As in (b) but for the response to sea surface warming. In (c), the dashed line shows the Clausius-Clapeyron approximation of the MSE increase. (d–f) As in (a–c) but for the negative of the MSE and DSE meridional gradients. The solid lines indicate statistically significant responses and the shading shows the inter-model spread.

The models agree well on the surface DSE and MSE responses to sea surface warming (Figure 1c). It is important to note that the models are forced by a structured SST perturbation and do not have imposed surface land temperature. All models show a meridionally uniform DSE increase of about $1.4 \, \text{kJ kg}^{-1}$ even over the Arctic where there is no SST forcing. The surface MSE response is quite different from the DSE signal. All models show a strong tropical surface MSE response to sea surface warming. This increase in latent heat follows nicely Clausius-Clapeyron scaling (Held & Soden, 2006, see dashed line in Figure 1c).

The response of the surface meridional MSE gradient (kJ/kg/°) due to Arctic sea ice loss (Figure 1e) indicates considerable weakening between 65°N and 85°N due to sea ice loss and consequent surface Arctic amplification (for reference, the climatology is shown in Figure 1d). A weakening in the surface MSE gradient is usually associated with less baroclinicity in the regions where the gradient weakens, which previous studies link to a decrease in eddy heat flux (Armour et al., 2019; Shaw & Voigt, 2016; Wu et al., 2011). The model spread in this response is evident poleward of 70°N, but the models align well equatorward of this latitude. In response to sea surface warming (Figure 1f), the MSE gradient strengthens quite uniformly over the whole Northern hemisphere (Shaw & Voigt, 2016).

3.2. Eddy PHT

We now focus on how sea ice loss and sea surface warming affect the climatological DSE and MSE transports (shown in Figure 2a) and the climatological vertical structure of the local eddy DSE and MSE flux (Figures 2d and 2h). Arctic sea ice loss decreases the net eddy PHT into the Arctic (Figure 2b). The models agree well on the location and amplitude of the dry and moist PHT response (see Figure S5 for the individual models), the multi-model mean showing a maximal decrease in moist PHT of 0.08 PW (0.06 PW per degree of global warming) with an inter-model spread of at most 0.04 PW. Reduction in eddy PHT is stronger during the boreal autumn and winter (see Figure S4), principally due to the stronger SIC forcing in boreal autumn that affects the eddies in boreal winter, the season when eddy PHT is strongest (Shaw & Voigt, 2016). The response to sea ice loss is mainly located at high latitudes but extends to the mid-latitudes, although not too far equatorward of the maximal sea ice extent (see Figure 2b). The eddy PHT response to
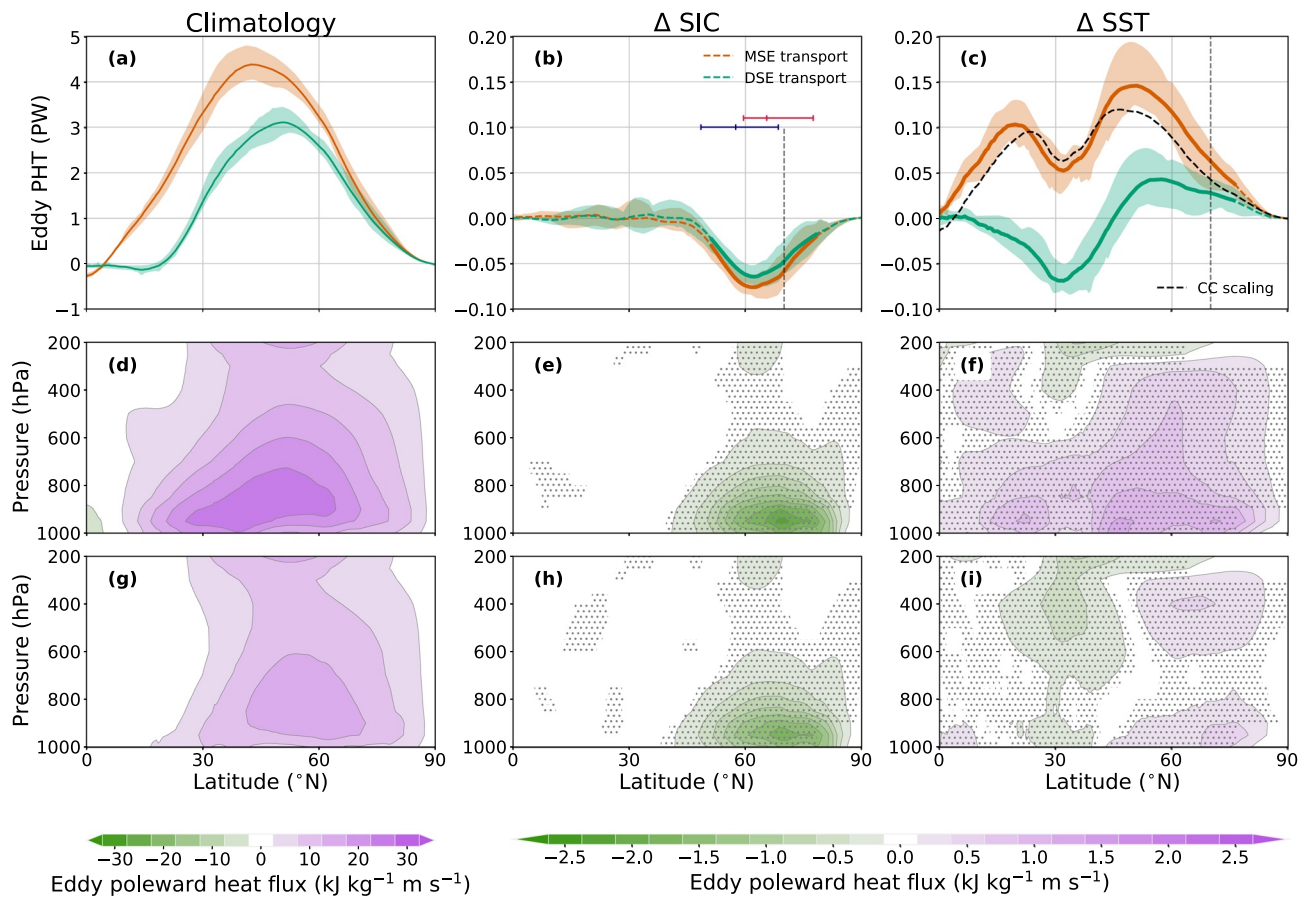
Figure 2. Eddy PHT in the PAMIP experiments. (a) Climatological multi-model average eddy PHT (orange is MSE transport and green is DSE transport) for the control experiment. (b) Eddy PHT response to Arctic sea ice loss. (c) Eddy PHT response to sea surface warming. The dashed black line is the Clausius-Clapeyron scaling for the MSE transport response. In panels (a,b,c), the model ensemble spread is shown in the shading around the curves. (d) Annual, zonal multi-model mean poleward eddy MSE flux. (e) Changes to the eddy flux of MSE in response to Arctic sea ice loss. (f) As in panel (e), for the response to sea surface warming. (g–i) as in (d–f) but for the poleward eddy DSE flux. The solid lines and stippling indicate statistical significance at a 95% confidence level. The 70°N latitude is highlighted with the gray dashed line. The sea ice extent is shown in (b) as in Figure 1b.

Arctic sea ice loss is consistently dominated by the reduction of dry eddy PHT with a reduction in eddy DSE (MSE) transport of 0.047 (0.058) PW at 70°N. In Section 3.1, we noted the disagreement in the intensity of the Arctic amplification signal between the models. Our results here suggest that this disagreement does not seem to be directly linked to the eddy PHT response but might be related to other, model-dependent factors.

The eddy PHT response to sea surface warming is dominated by the response in latent eddy PHT (Figure 2c) and exhibits a distinct camelback meridional structure with two maxima around 20°N and 50°N with a local minimum south of 30°N. As for the MSE response, the response in the eddy MSE flux closely follows the Clausius-Clapeyron relation with the temperature and specific humidity taken locally (Held & Soden, 2006, black dashed line in Figure 2c). This simple scaling relates the increase in moisture content and moisture transport to surface warming, assuming fixed relative humidity conditions. The models agree relatively well in the tropics and the extra-tropics, but north of 45°N the inter-model spread increases considerably, up to 0.08 PW. This disagreement in the magnitude of the response comes from the dry eddy PHT response (green line); the models agree well on the latent eddy PHT even where the inter-model spread is the largest. Into the Arctic, at 70°N, the eddy DSE transport is relatively small (0.028 PW) compared to the eddy MSE transport (0.063 PW). The response to sea surface warming is more complex and model dependent. The signal in the northern hemisphere maximizes during boreal winter due to the intensification of the eddies, the climatological eddy PHT being at its maximum during this season (see Figure S5).

Responses to Arctic sea ice loss and sea surface warming have a similar intensity but with opposite sign at high latitudes. This opposition in the responses leads to a significantly weaker eddy MSE transport (0.005 PW at 70°N, not shown) when summing both responses. This small net eddy MSE transport comes from a large latent heat transport mainly from the sea surface warming (0.024 PW) compared to the reduction of eddy DSE transport principally from sea ice loss (−0.020 PW).

The multi-model mean climatological eddy MSE flux ($\overline{\left[v^* MSE^* \right]}$, Figure 2d) reaches its maximum near the surface at 40°N, spans over the whole troposphere and reaches the stratosphere. The eddy DSE flux climatology (Figure 2g) resembles the eddy MSE flux but with an intensity of about half the strength of the MSE flux and with a maximum shifted to about 55°N. In response to Arctic sea ice loss, the eddy MSE flux shows a weakening at high latitudes (Figure 2e). The annual mean signal is confined to the lower troposphere with a maximum located at 70°N near the surface, which is consistent with previous studies (Deser et al., 2010; Kay et al., 2012). The response is dominated by the eddy DSE flux response (Figure 2h). There are multiple mechanistic interpretations of this reduction of northward eddy heat flux. It could come about as a decrease in equatorward transport of anomalously cold air in the form of weaker (warmer) or less frequent cold air outbreaks (Ayarzagüena & Screen, 2016) but we will argue below that it is best interpreted as an increase in equatorward transport of anomalously warm air. In response to sea surface warming, the eddy MSE flux response acts to intensify the climatological heat flux (Figure 2f). The eddy DSE flux response is weaker, the eddy MSE flux response coming primarily from an increase in meridional eddy latent heat flux reaching up to 4% per degree of global warming. The magnitude of the response to sea surface warming is, locally, about three times less than the response to Arctic sea ice loss, but dominates at higher altitude as the signal is not confined to the lower troposphere.

3.3. Response of the Moist Isentropic Circulation

Figure 3a shows the eddy mass streamfunction on MSE levels (ψ_E) calculated using the STEM, defined positive clockwise here. The circulation represented by ψ_E describes a clockwise circulation in this latitude-MSE space, with upward (downward) motions representing heating (cooling) and rightward (leftward) motions representing northward (southward) displacements.

The responses of the multi-model mean ψ_E to Arctic sea ice loss and sea surface warming are shown in Figures 3b and 3c, respectively. The eddy streamfunction is shown here because it dominates the total climatological streamfunction and its response. Changes to the mean circulation associated with sea ice loss and sea surface warming are much weaker than those of the eddy circulation (checked but not shown).

The returning branch of the streamfunction at high-latitudes weakens by up to 5% (about 3.6% per degree of global warming) in response to Arctic sea ice loss. The eddy streamfunction responds very differently to sea surface warming compared to Arctic sea ice loss. The magnitude of the response to sea surface warming is about 10 times larger than the response to sea ice loss (note the different scales in Figures 3a and 3b). The dipole structure of the response indicates a shift of the circulation to higher MSE levels and reaches up to 13% of the total signal (9.2% per degree of global warming).

The annually averaged multi-model mean eddy PHT is shown in Figure 3d along with the contributions of the poleward and equatorward branches of the moist isentropic circulation. Both branches transport heat poleward and equatorward with transport values on the order of 50 PW but largely cancel, leading to a net eddy PHT on the order of a few PW.

In Figures 3e and 3f, the multi-model mean eddy PHT response is separated into three components: the change from the eddy mass flux (δF_E), the change in the mean h^+ in the upper branch (δh^+), and the change in the mean h^- in the lower branch (δh^-); see Section 2.2 for details. In response to Arctic sea ice loss (Figure 3e), the contribution of the mass transport (black dashed-dotted line) is weak and of mixed sign compared to the contribution of the changes in effective stratification (black dotted line). The black dotted line is the sum of the orange and green dotted lines. Additionally, the largest part of the effective stratification contribution comes from the warming of the equatorward branch at high latitudes (dotted green line), resulting in an increase in the equatorward heat transport and expressed as a reduction in eddy PHT in Figure 2b. In response to sea surface warming, the mass transport changes play a dominant role north of 45°N while the
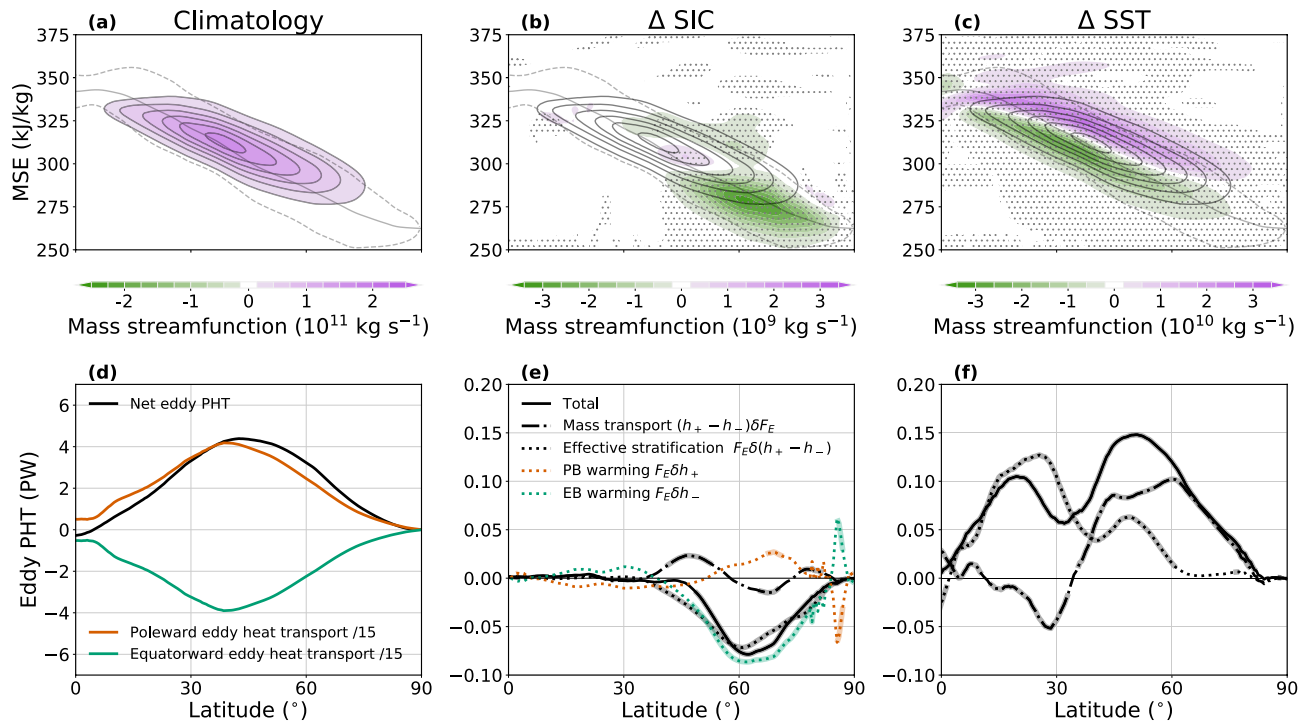
Figure 3. The ensemble average annual mean eddy PHT. (a) Multi-model average of the annual mean eddy mass streamfunction on MSE levels and annual mean zonal mean surface MSE (solid gray line) with ± two standard deviations (dashed gray lines). (b) Response of the eddy mass streamfunction to imposed Arctic sea ice loss. (c) As in (b) but in response to sea surface warming. In panels (b) and (c), the climatology of the control experiment is shown in contours (contour interval 2.5×10^{10} kg s^{-1}). (d) Ensemble average annual mean eddy PHT (black), PHT due to the poleward branch (red) and PHT due to the equatorward branch (green); the contributions of the individual branches have been divided by 15 to show on the same axis. (e) Eddy PHT response (black solid) to Arctic sea ice loss decomposed into mass transport effect (dashed-dot), effective stratification (black-dotted), warming of poleward branch (PB warming, orange-dotted) and warming of equatorward branch (EB warming, green-dotted). (f) As in (e) but in response to sea surface warming. The contribution of the individual branches is not shown for clarity. The stippling in the top row indicates statistical significance at a 95% confidence level. In panels (e) and (f), statistical significance is indicated by the thicker lines.

effect of the effective stratication changes dominates south of 45°N. Because of the large compensation of the changes of the effective temperature of both branches (the orange and green dotted lines) the change in effective stratification does not greatly impact the eddy PHT. For clarity, these two lines are not shown in Figure 3f as they are an order of magnitude larger and cancel out into the black dotted line. Our results are also broadly consistent with Shaw et al. (2018) who used an energy budget approach to link changes to eddy PHT to surface turbulent heat fluxes (see Figure S5 and discussion in supporting information)

Overall, there is a clear distinction at high latitudes between the eddy PHT response to Arctic sea ice loss and to sea surface warming. The former is primarily a thermodynamic response and the latter is primarily a dynamical response. This result shows that the heat and the mass transport do not respond in the same way. Although the changes in the eddy PHT follow the changes in the meridional MSE gradient, the eddy mass transport response does not. In fact, in response to sea ice loss, the eddy mass transport does not change much and the changes in PHT come from a change in the amount of heat that these waves transport, rather than a weakening of the eddies.

4. Conclusions

We have demonstrated the opposite responses of eddy PHT to sea surface warming and Arctic sea ice loss in PAMIP. Arctic sea ice loss that is consistent with 1.4°C of global warming increases the equatorward eddy heat transport out of the Arctic (at 70°N) by 0.058 PW (or 0.041 PW per degree Celsius). This increase in heat transport primarily comes from a warming of the equatorward flow at high latitudes with a small contribution from a weakening of the eddy mass transport. Conversely, warming the SST increases eddy PHT into the Arctic by 0.063 PW (0.045 PW per degree Celsius), an increase mostly due to a strengthening of the eddy

mass transport at high latitudes. However, owing primarily to the inter-model spread in dry eddy PHT, the response to sea surface warming is less robust than to Arctic sea ice loss. These opposite responses exhibit a similar cancellation as presented by Hwang et al. (2011) but are here explicitly linked to sea ice loss and low-latitude sea surface warming effects in a range of AGCM components of state-of-the-art earth system models. We have also shown how these changes in eddy PHT can be explained by the changes in the moist isentropic circulation, including a warming of the returning branch at high latitudes in response to sea ice loss and an overall strengthening of the circulation in response to sea surface warming.

This study highlights the strong agreement between several models participating in PAMIP in the eddy PHT and moist isentropic circulation responses to sea ice loss regardless of the discrepancy in the amplitude of their respective polar amplification signal. Examination of the mechanisms driving the spread in polar amplification should be the focus of future work related to PAMIP. The reason that the PHT response to sea ice loss is more robust than the PHT response to tropical warming should also be examined. This robustness is however less present for the PHT response to sea surface warming. It also remains to investigate how the PAMIP models respond in the presence of coupled ocean-atmosphere interactions, knowing that oceanic heat transport and local and nonlocal feedbacks could potentially play a large role (Deser et al., 2016; Kay et al., 2012; Tomas et al., 2016). Higher-tier experiments in the PAMIP protocol will be conducted to assess the effect of coupling.

Data Availability Statement

The data are available through the following link https://doi.org/10.5683/SP2/Z6GVH1.

References

Alexeev, V. A., & Jackson, C. H. (2013). Polar amplification: Is atmospheric heat transport important? *Climate Dynamics*, *41*(2), 533–547. https://doi.org/10.1007/s00382-012-1601-z

Armour, K. C., Siler, N., Donohoe, A., & Roe, G. H. (2019). Meridional atmospheric heat transport constrained by energetics and mediated by large-scale diffusion. *Journal of Climate*, *32*(12), 3655–3680. https://doi.org/10.1175/JCLI-D-18-0563.1

Ayarzagüena, B., & Screen, J. A. (2016). Future Arctic sea ice loss reduces severity of cold air outbreaks in mid-latitudes. *Geophysical Research Letters*, *43*(6), 2801–2809. https://doi.org/10.1002/2016GL068092

Barpanda, P., & Shaw, T. A. (2020). Surface fluxes modulate the seasonality of zonal-mean storm tracks. *Journal of the Atmospheric Sciences*, *77*(2), 753–779. https://doi.org/10.1175/jas-d-19-0139.1

Caballero, R., & Langen, P. L. (2005). The dynamic range of poleward energy transport in an atmospheric general circulation model. *Geophysical Research Letters*, *32*(2). https://doi.org/10.1029/2004GL021581

Czaja, A., & Marshall, J. (2006). The partitioning of poleward heat transport between the atmosphere and ocean. *Journal of the Atmospheric Sciences*, *63*(5), 1498–1511. https://doi.org/10.1175/JAS3695.1

Deser, C., Sun, L., Tomas, R. A., & Screen, J. (2016). Does ocean coupling matter for the northern extratropical response to projected Arctic sea ice loss? *Geophysical Research Letters*, *43*(5), 2149–2157. https://doi.org/10.1002/2016GL067792

Deser, C., Tomas, R., Alexander, M., & Lawrence, D. (2010). The seasonal atmospheric response to projected Arctic Sea ice loss in the late twenty-first century. *Journal of Climate*, *23*(2), 333–351. https://doi.org/10.1175/2009JCLI3053.1

Döös, K., & Nilsson, J. (2011). Analysis of the meridional energy transport by atmospheric overturning circulations. *Journal of the Atmospheric Sciences*, *68*(8), 1806–1820. https://doi.org/10.1175/2010JAS3493.1

Eyring, V., Bony, S., Meehl, G. A., Senior, C. A., Stevens, B., Stouffer, R. J., & Taylor, K. E. (2016). Overview of the Coupled Model Intercomparison Project Phase 6 (CMIP6) experimental design and organization. *Geoscientific Model Development*, *9*(5), 1937–1958. https://doi.org/10.5194/gmd-9-1937-2016

Fajber, R., Kushner, P. J., & Laliberté, F. (2018). Influence of mid-latitude surface thermal anomalies on the polar midtroposphere in an idealized moist model. *Journal of the Atmospheric Sciences*, *75*(4), 1089–1104. https://doi.org/10.1175/JAS-D-17-0283.1

Frierson, D. M. W., Held, I. M., & Zurita-Gotor, P. (2007). A gray-radiation aquaplanet moist GCM. Part II: Energy transports in altered climates. *Journal of the Atmospheric Sciences*, *64*(5), 1680–1693. https://doi.org/10.1175/JAS3913.1

Golaz, J.-C., Caldwell, P. M., Roekel, L. P. V., Petersen, M. R., Tang, Q., Wolfe, J. D., & Zhu, Q. (2019). The DOE E3SM coupled model Version 1: Overview and evaluation at standard resolution. *Journal of Advances in Modeling Earth Systems*, *11*(7), 2089–2129. https://doi.org/10.1029/2018MS001603

Hartmann, D. L., & Ceppi, P. (2014). Trends in the CERES dataset, 2000-13: The effects of sea ice and jet shifts and comparison to climate models. *Journal of Climate*, *27*(6), 2444–2456. https://doi.org/10.1175/JCLI-D-13-00411.1

Held, I. M. (2001). The partitioning of the poleward energy transport between the tropical ocean and atmosphere. *Journal of the Atmospheric Sciences*, *58*(8), 943–948. https://doi.org/10.1175/1520-0469(2001)058⟨0943:TPOTPE⟩2.0.CO;

Held, I. M., & Soden, B. J. (2006). Robust responses of the hydrological cycle to global warming. *Journal of Climate*, *19*(21), 5686–5699. https://doi.org/10.1175/jcli3990.1

Hewitt, H. T., Copsey, D., Culverwell, I. D., Harris, C. M., Hill, R. S. R., Keen, A. B., et al. (2011). Design and implementation of the infrastructure of hadgem3: The next-generation met office climate modeling system. *Geoscientific Model Development*, *4*(2), 223–253. https://doi.org/10.5194/gmd-4-223-2011

Hwang, Y.-T., & Frierson, D. M. W. (2010). Increasing atmospheric poleward energy transport with global warming. *Geophysical Research Letters*, *37*(24). https://doi.org/10.1029/2010GL045440

Hwang, Y.-T., Frierson, D. M. W., & Kay, J. E. (2011). Coupling between Arctic feedbacks and changes in poleward energy transport. *Geophysical Research Letters*, *38*(17). https://doi.org/10.1029/2011GL048546

Kay, J. E., Holland, M. M., Bitz, C. M., Blanchard-Wrigglesworth, E., Gettelman, A., Conley, A., & Bailey, D. (2012). The influence of local feedbacks and northward heat transport on the equilibrium Arctic climate response to increased greenhouse gas forcing. *Journal of Climate*, *25*(16), 5433–5450. https://doi.org/10.1175/JCLI-D-11-00622.1

Kim, D., Kang, S. M., Shin, Y., & Feldl, N. (2018). Sensitivity of polar amplification to varying insolation conditions. *Journal of Climate*, *31*(12), 4933–4947. https://doi.org/10.1175/jcli-d-17-0627.1

Laliberté, F., Shaw, T., & Pauluis, O. (2012). Moist recirculation and water vapor transport on dry isentropes*. *Journal of the Atmospheric Sciences*, *69*(3), 875–890. https://doi.org/10.1175/jas-d-11-0124.1

Lauritzen, P. H., Nair, R. D., Herrington, A. R., Callaghan, P., Goldhaber, S., Dennis, J. M., et al. (2018). NCAR release of CAM-SE in CESM2.0: A reformulation of the spectral element dynamical core in dry-mass vertical coordinates with comprehensive treatment of condensates and energy. *Journal of Advances in Modeling Earth Systems*, *10*(7), 1537–1570. https://doi.org/10.1029/2017MS001257

Marsh, D. R., Mills, M. J., Kinnison, D. E., Lamarque, J.-F., Calvo, N., & Polvani, L. M. (2013). Climate change from 1850 to 2005 simulated in CESM1(WACCM). *Journal of Climate*, *26*(19), 7372–7391. https://doi.org/10.1175/JCLI-D-12-00558.1

Pauluis, O., Czaja, A., & Korty, R. (2010). The global atmospheric circulation in moist isentropic coordinates. *Journal of Climate*, *23*(11), 3077–3093. https://doi.org/10.1175/2009JCLI2789.1

Pauluis, O., Shaw, T., & Laliberté, F. (2011). A statistical generalization of the transformed Eulerian-mean circulation for an arbitrary vertical coordinate system. *Journal of the Atmospheric Sciences*, *68*(8), 1766–1783. https://doi.org/10.1175/2011JAS3711.1

Screen, J. A., Simmonds, I., Deser, C., & Tomas, R. (2013). The atmospheric response to three decades of observed Arctic Sea ice loss. *Journal of Climate*, *26*(4), 1230–1248. https://doi.org/10.1175/JCLI-D-12-00063.1

Shaw, T. A., Barpanda, P., & Donohoe, A. (2018). A moist static energy framework for zonal-mean storm-track intensity. *Journal of the Atmospheric Sciences*, *75*(6), 1979–1994. https://doi.org/10.1175/jas-d-17-0183.1

Shaw, T. A., & Tan, Z. (2018). Testing latitudinally dependent explanations of the circulation response to increased CO_2 using aquaplanet models. *Geophysical Research Letters*, *45*(18), 9861–9869. https://doi.org/10.1029/2018gl078974

Shaw, T. A., & Voigt, A. (2016). What can moist thermodynamics tell us about circulation shifts in response to uniform warming? *Geophysical Research Letters*, *43*(9), 4566–4575. https://doi.org/10.1002/2016GL068712

Smith, D. M., Screen, J. A., Deser, C., Cohen, J., Fyfe, J. C., García-Serrano, J., et al. (2019). The Polar Amplification Model Intercomparison Project (PAMIP) contribution to CMIP6: Investigating the causes and consequences of polar amplification. *Geoscientific Model Development*, *12*(3), 1139–1164. https://doi.org/10.5194/gmd-12-1139-2019

Stevens, B., Giorgetta, M., Esch, M., Mauritsen, T., Crueger, T., Rast, S., et al. (2013). Atmospheric component of the MPI-M Earth System Model: ECHAM6. *Journal of Advances in Modeling Earth Systems*, *5*(2), 146–172. https://doi.org/10.1002/jame.20015

Stuecker, M. F., Bitz, C. M., Armour, K. C., Proistosescu, C., Kang, S. M., Xie, S.-P., et al. (2018). Polar amplification dominated by local forcing and feedbacks. *Nature Climate Change*, *8*(12), 1076–1081. https://doi.org/10.1038/s41558-018-0339-y

Swart, N. C., Cole, J. N. S., Kharin, V. V., Lazare, M., Scinocca, J. F., Gillett, N. P., & Winter, B. (2019). The Canadian Earth System Model version 5 (CanESM5.0.3). *Geoscientific Model Development Discussions*, 1–68. https://doi.org/10.5194/gmd-2019-177

Tomas, R. A., Deser, C., & Sun, L. (2016). The role of ocean heat transport in the global climate response to projected Arctic Sea ice loss. *Journal of Climate*, *29*(19), 6841–6859. https://doi.org/10.1175/JCLI-D-15-0651.1

Trenberth, K. E., & Stepaniak, D. P. (2003). Covariability of components of poleward atmospheric energy transports on seasonal and interannual timescales. *Journal of Climate*, *16*(22), 3691–3705. https://doi.org/10.1175/1520-0442(2003)016⟨3691:COCOPA⟩2.0.CO;2

Vallis, G. K., Zurita-Gotor, P., Cairns, C., & Kidston, J. (2015). Response of the large-scale structure of the atmosphere to global warming. *Quarterly Journal of the Royal Meteorological Society*, *141*(690), 1479–1501. https://doi.org/10.1002/qj.2456

Wu, Y., & Pauluis, O. (2013). Examination of isentropic circulation response to a doubling of carbon dioxide using statistical transformed eulerian mean*. *Journal of the Atmospheric Sciences*, *70*(6), 1649–1667. https://doi.org/10.1175/JAS-D-12-0235.1

Wu, Y., Ting, M., Seager, R., Huang, H.-P., & Cane, M. A. (2011). Changes in storm tracks and energy transports in a warmer climate simulated by the GFDL CM2.1 model. *Climate Dynamics*, *37*(1), 53–72. https://doi.org/10.1007/s00382-010-0776-4